

Electron-Positron pairs creation close to a black hole horizon. Red-shifted annihilation line in the emergent X-ray spectra of a black hole, part I

PHILIPPE LAURENT^{1,2} AND LEV TITARCHUK³

¹*CEA/DRF/IRFU/DAP, CEA Saclay, 91191 Gif sur Yvette, France; philippe.laurent@cea.fr*

²*Laboratoire APC, 10, rue Alice Domon et Léonie Duquet, 75205 Paris Cedex 13, France*

³*Dipartimento di Fisica, Università di Ferrara, Via Saragat 1, I-44100 Ferrara, Italy; titarchuk@fe.infn.it*

(Received January 1, 2018; Revised October 28, 2021; Accepted April 22, 2018)

Submitted to ApJ

ABSTRACT

We consider a Compton cloud (CC) surrounding a black hole (BH) in an accreting black hole system, where electrons propagate with thermal and bulk velocities. In that cloud, soft (disk) photons may be upscattered off these energetic electrons and attain several MeV energies. They could then create pairs due to these photon-photon interactions. In this paper, we study the formation of the 511 keV annihilation line due to this photon-photon interaction, which results in the creation of electron-positron pairs, followed by the annihilation of the created positrons with the CC electrons. The appropriate conditions of annihilation line generation take place very close to a BH horizon within $(10^3 - 10^4)m$ cm from it, where m is the BH hole mass in solar units. As a result, the created annihilation line should be seen by the Earth observer as a blackbody bump, or so called reflection bump at energies around $(511/20)(20/z)$ keV where $z \sim 20$ is a typical gravitational red-shift experienced by the created annihilation line photons when they emerge. This transient feature should occur in any accreting black hole systems, galactic or extragalactic. Observational evidences for this feature in several galactic black hole systems is detailed in an accompanying paper (II). An extended hard tail of the spectrum up to 1 MeV may be also formed due to X-ray photon upscattering off created pairs.

Keywords: Black hole physics - X-rays: general - radiation mechanism: non-thermal - relativistic processes

1. INTRODUCTION

Accreting stellar-mass black holes (BHs) in Galactic binaries exhibit high-soft and low-hard spectral states and transitions between them (the intermediate state; see details in [Shaposhnikov & Titarchuk \(2009\)](#), hereafter ST09). Usually an increase in the soft blackbody (BB) luminosity component leads to the appearance of an extended power law. However, the extension of the power law is not a monotonic function of the power law index. Using data of the *Rossi X-ray Time Explorer (RXTE)* for black hole candidate (BHC) XTE J1550-564 [Titarchuk & Shaposhnikov \(2010\)](#) demonstrate that efold energy E_{fold} of the spectra decreases when the photon index Γ increases starting from $\Gamma \sim 1.4$ and then, at some value of $\Gamma \sim 2.2$, it starts increasing towards energy of 200 keV. An important observational fact is that this effect is seen as a persistent phenomenon only in BH candidates, and thus it is apparently a unique BH signature. In neutron star (NS) sources, E_{fold} —energy gradually decreases towards the soft state [see e.g. [Seifina & Titarchuk \(2011\)](#) and [Titarchuk, Seifina & Frontera \(2013\)](#), hereafter TSF13]. Although in NSs, similar power law components are detected in the hard and intermediate states (hereafter the LHS and the IS, respectively) their extension becomes smaller (or E_{fold}) with increasing luminosity [see [Di Salvo \(2000\)](#) and [Farinelli & Titarchuk \(2011\)](#), hereafter FT11].

Moreover, ST09 find that photon index Γ saturates with the dimensionless mass accretion rate $\dot{m} = \dot{M}/\dot{M}_{crit}$ where $\dot{M}_{crit} = L_{Edd}/c^2$, with $L_{Edd} = 4\pi GMm_p c/\sigma_T$, is the Eddington luminosity, m_p the proton mass, σ_T the Thomson cross-section and c the speed of light. Naturally, the photon index Γ saturates with a quasi-periodic oscillation frequency (QPO) (and the mass accretion rate) in BH sources while FT11 and TSF13 demonstrate that Γ stays almost the same around 2 in NSs. Thus, it seems a reasonable assumption that we deal here with a unique spectral signature of BH binaries which is directly tied to the black hole event horizon.

In Laurent & Titarchuk (1999) (hereafter LT99), we suggested that the BH X-ray spectrum in the high soft state (HSS) is formed in a relatively cold accretion flow with a relativistic bulk velocity $v_{bulk} \sim c$ and with the plasma (electron) temperature of a few keV or less, for which the thermal electron velocity $v_{th} \ll c$. It is worth pointing out that in such a flow the effect of the bulk Comptonization is much stronger than the effect of the thermal Comptonization which is a second order with respect to v_{th}/c (LT99). Very close to the horizon, X-ray photons can be up-scattered by bulk electrons to very high energies, of order 1 MeV and higher but the observer on Earth will see these up-scattered photons at lower energies, of the order of 300 – 400 keV, because of gravitational redshift.

Using Monte Carlo simulations, LT99 compute X-ray spectra of such BH sources. They take into account up-scattering of the soft (disk) photons illuminating the Compton cloud (CC) and they implement the full relativistic treatment to reproduce these spectra. The resulting spectra obtained using this treatment can be described as a sum of a thermal (disk) component and the convolution of some fraction of this component with the CC upscattering spread (Green's) function. The upscattered part of the spectrum is seen as an extended power law over energies much higher than the characteristic energy of the soft photons. LT99 show that the photon index Γ increases with an increase of the mass accretion rate and then it stabilizes at $\Gamma = 2.8 \pm 0.1$, similarly to what was observed by ST09. This index stability occurs over a wide range of the plasma temperature, 0 – 10 keV, and dimensionless mass accretion rates \dot{m} (higher than 2 in Eddington units).

LT99 also demonstrate that the sharp high-energy cutoff occurs at energies of 200-400 keV, which are related to the average energy of electrons, $m_e c^2$ impinging on the event horizon. Although, the spectrum is practically identical to the standard thermal Comptonization spectrum [see e.g. Hua & Titarchuk (1995)] when the CC plasma temperature is getting of order of 50 keV (the typical ones for the hard state of BH). In this case, one can only see the effect of the bulk motion at high energies, where there is an excess in the spectrum with respect to the pure thermal one. Furthermore, LT99 demonstrate that the change of spectral shape from the soft X-ray state to the hard X-ray state is clearly to be related to the Compton cloud temperature. Indeed, the effect of the bulk Comptonization compared with the thermal one is getting stronger when the plasma temperature drops below 10 keV.

Furthermore, Laurent & Titarchuk (2001), hereafter LT01, show that the high-energy photon production (source function) is distributed with the characteristic maximum at about the photon bending radius $1.5r_S$, where $r_S = 2GM/c^2$ is the Schwarzschild radius and M is a BH mass, independently of the seed (soft) photon distribution. Most of these photons fall down then into the black hole, but some of them anyway have time to interact with another X-ray photon by photon-photon process to make an electron-positron pairs (Svensson 1982). In this paper, we explore in details the consequences of this pair creation process which occurs very close to a BH horizon, $(10^3 - 10^4)m$ cm from it (m is the BH hole mass in solar units) and we elaborate the observational consequences of this effect.

In the next section, we proceed with the details of the Monte Carlo simulations of the upscattering of the soft (disk) photons in the converging flow, and of the pair creation due to the interaction of these up-scattered photons with unscattered X-ray photons in the close vicinity of a BH horizon. Then, we explore in details the observational consequences of this effect. In the Appendix, we give an analytical derivation of some key results obtained through the simulations.

2. THE MONTE-CARLO SIMULATIONS

The geometry used in these simulations is similar to the one used in LT99, consisting of a thin disk with an inner radius of $3r_S$, merged with a spherical Compton Cloud (CC) harboring a BH in its center. The CC outer radius is r_{out} . The disk is assumed always to be optically thick. In addition to the free-fall into the central BH, with a bulk velocity of the infalling plasma given by $v(r) = c(r_S/r)^{1/2}$, where r_S is the Schwarzschild radius (Titarchuk, Mastichiadis & Kylafis (1997)), we have also taken into account the thermal motion of the CC electrons, simulated in most of the results shown here at an electron temperature of 5 keV, a typical temperature of the CC in the high-soft state of galactic BHs (see Fig. 1). The CC temperature is less than the temperature of the sub-Keplerian inflow (presumably located

above the disk) but it is higher than the temperature of the disk flow which is of order of a few keV or less (e.g. Shakura & Sunyaev (1973)).

The seed X-ray photons were generated uniformly and isotropically at the surface of the border of the accretion disk, from $r_{d,in} = 3r_S$ to $r_{d,out} = 10r_S$. These photons were generated according to a thermal spectrum with a single temperature of 0.9 keV, similar to the ones measured in black hole binary systems (see for example Borozdin et al. (1999)). To reach a satisfying statistic level for our computations, we made simulations using 10^9 seed (disk) photons.

In Figure 1 we present a geometry of X-ray spectral formation in BH source. Soft X-ray photons coming from the disk illuminate the Compton cloud and its innermost part, where the bulk velocity is dominating in the converging flow (CF) region). These photons upscatter off electrons in these configurations and some part of these photons come to the observer, seen as a specific Comptonization spectrum.

In our simulations [see also the kinetic formalism in Titarchuk & Zannias (1998), hereafter TZ98] we use the number density n_{ff} of the flow measured in the laboratory frame of the flow $n_{ff} = \dot{m}(r_S/r)^{1/2}/(2R\sigma_T)$. Here $\dot{m} = \dot{M}/\dot{M}_{Edd}$, \dot{M} is the mass accretion rate, σ_T is the Thomson cross section, and $\dot{M}_E \equiv L_{Edd}/c^2 = 4\pi GMm_p/\sigma_T c$ is the Eddington accretion rate. The parameters of our simulations are thus, the BH mass m in solar units, the CC electron temperature, T_e , the mass accretion rate, \dot{m} , and the CC outer radius, $r_{out} = 10r_S$. The cloud Thomson optical thickness is expressed through the mass accretion rate \dot{m} according to the following formulae (see e.g. TZ98) :

$$\tau_{ff} = \frac{\dot{m}}{2} \int_1^{x_{out}} \frac{dx}{x^{3/2}\sqrt{1-x^{-1}}} = \dot{m} \left(\frac{\pi}{2} - \arcsin \sqrt{\frac{r_s}{r_{out}}} \right) \quad (1)$$

where $x_{out} = r_{out}/r_S$.

In Figure 2, we show the average photon energy of the upscattered photons (black histogram) and blue-shifted energy of injected soft photon (blue line) as a function of radius. As one can see, the injected (disk) photons illuminating in the CF innermost region are strongly blue-shifted; at 30 meters from a BH horizon (for a 10 solar masses BH) their energy is of order of few MeV. One should keep in mind however that only a few of these photons can directly reach a BH horizon when the accretion rate is high (in the HSS) as the CF optical depth $\tau_{ff} \gg 1$ for $\dot{m} \gg 1$ (see Eq. 1). In addition to the Compton effect, we compute the probability of making a pair, using the pair creation cross section given by Svensson (1982). The kinetic properties of the pair are computed in the local rest frame using standard formulae, derived from the energy and momenta conservation, and the results stored in a file for a subsequent treatment. The created pair properties are described below. Afterward, using another Monte-Carlo simulation, we propagate the pairs in the Schwarzschild metric, slowing them down by Coulomb scattering, and checking if the positrons annihilate or not. The resulting annihilation photons were also tracked by a third Monte-Carlo in the CC, to see if they escape or are scattered off due to the CC optical depth.

3. CREATED PAIRS PROPERTIES

As one can see from Fig. 3, the pairs are produced in the Monte-Carlo simulations very close to a BH horizon. For a ten solar masses black hole, this creation occurs even at a few hundred meters away from the horizon. This result is confirmed by computations given in Appendix.

The pair creation process depends on the properties of the background X-ray photons, and, in particular, of the source X-ray luminosity. Then we have simulated the pairs creation process for different value of the source X-ray luminosity and computed for each of them the number of positrons created close to the black hole. These numbers are presented in Figs. 4-5 for the low/hard and the high/soft states, respectively. We choose these two BH spectral states in order to demonstrate a trend in the creation of positron number as a function of the luminosity for two cases of the model parameters, the plasma temperature, kT_e and \dot{m} , even if these states does not span on their own the whole luminosity range. We should point out that although the two curves are similar each other, the low-hard state (LHS) plot is situated a factor five below the high-soft state (HSS) one. This is mainly due to the difference in the mass accretion rate \dot{m} between these two cases. This linear dependence of the number of the created pairs on \dot{m} occurs when the luminosity reaches 10^{36} erg/s, when the number of created positrons is equal to around $10^5 L_X$ and $5 \times 10^5 L_X$ for the LH and HS states, respectively (see Figures 4–5). Simulations also show that, independently of the source X-ray luminosity, the positron kinetic energy spectrum remains nearly the same.

4. THE EMERGENT PHOTON SPECTRUM OF AN ACCRETING BLACK HOLE

4.1. A redshifted 511 keV annihilation line feature

As we have already discussed, the pair creation occurs very close to the horizon, of the order of 100 meters from the the horizon for a 10 solar mass BH. In Figure 6, we show the trajectories of the created positrons in the Schwartzchild background. It can be seen that only a few of them, among the 5×10^5 positrons simulated to produce this Figure, can reach $3 r_s$. This number is even lower if we take into account Coulomb losses and the pair annihilation process.

Having the results of our first Monte-Carlo, we have built another Monte-Carlo software with which we simulate the propagation of the created positrons in the cloud, taking into account energy losses due to Coulomb scattering with protons. This process is the dominant cooling one, considering the physical condition of the cloud (see discussion in Moskalenko & Jourdain (1997)). We compute also the annihilation probability for positrons, and check for each positron if it annihilates or not. If the annihilation occurs then we store the kinetic energy and location of this positron at the moment of the annihilation. If not, these positrons can either fall into a BH, Compton scatter off background photons, escape from the system or annihilate further away, outside the CC, depending on the density of the surrounding material at several Schwartzchild radii. If we suppose that all positrons escaping from the CC annihilate afterward, the maximum expected 511 keV photon flux is around 10^{36} photon/s (i.e. 10^{30} erg/s) for a luminosity of 10^{38} erg/s. In a further step, we derive, using a third Monte-Carlo code and the saved annihilated positrons locations, the emergent annihilation radiation. As the 511 keV annihilation emission is produced at different radius from the BH, the line endures different redshifts, depending on the location of the annihilation and thus, this annihilation process shows up to the external observer as a specific continuum. In Figure 7, we show the resulting spectra for a CC electron temperature of 5 keV. In this set of simulations, \dot{m} was set equal to 1 (blue line), 4 (red line), and 10 (green line). The spectrum become harder as \dot{m} increases. Also, due to the concurring effects of the pair creation efficiency, which increases with \dot{m} , and CC opacity to the 511 keV radiation, decreasing with \dot{m} , we could see in Figure 7 that the spectrum is maximum for intermediate values of $\dot{m} = 4$.

Then we have explored what happens if we keep constant the mass accretion rate ($\dot{m} = 4$), while varying the CC electron temperature. The result can be seen in Figure 8, where we present the emergent annihilation spectrum with a CC electron temperature of 5 keV (blue line) and 50 keV (red line). One can notice that the overall spectrum shape does not change much except that the spectrum shift toward higher energies when we increase the cloud temperature, kT_e .

In Figure 9, we show also the emergent Comptonized spectrum of the CC, with an electron temperature of $kT_e = 5$ keV, including the gravitationally redshifted annihilated line. On the upper encapsulated right-hand panel, we include the redshifted annihilation line as a ratio of the resulting spectral values to the Comptonized continuum. These simulations show that the emergent annihilation spectrum is quasi-universal whatever the CC physical conditions are. In Figures 7-8, we demonstrate also that these redshifted annihilation lines can be represented by a blackbody-like shape, as shown by the dash lines which gives the blackbody best fit for the $\dot{m} = 1$ and $\dot{m} = 4$ case respectively.

However, observationally, this feature should be transient and cannot be observed in all black hole spectral states. Indeed, if the resulting X-ray luminosities $L_\gamma \gg 10^{37} (M_{bh}/10M_\odot)$ erg/s, the dimensionless mass accretion rate (see Titarchuk & Zannias (1998)) is much greater than 1, and the produced pairs and annihilation photons generated near a BH horizon cannot escape, as they are effectively scattered off converging electrons. In the LHS we cannot see the HBB either, and consequently the redshifted annihilation line, because $\tau_{\gamma-\gamma} \ll 1$ and pairs are not effectively generated. Moreover, in LHS, the converging flow is surrounded by a hot, relatively thick Compton Cloud (CC) with plasma temperature of order of 50-80 keV. Thus, the escaping HBB photons are scattered off hot electrons of the CC and the bump is smeared out. So, we expect this feature to be seen only during the IS when the mass accretion rate is sufficient to trigger the effect but no strong enough to hide it afterward.

4.2. Emergent spectrum taking into account the pair creation

In the previous section, we demonstrated that the pairs are created very close to horizon due to photon-photon interactions. In fact, these photons reach the necessary conditions for the pair creation when the product of their energies $E_1 E_2 > (m_e c^2)^2$. In Figure 10, we show the redshifted annihilation line and the classical bulk motion Comptonization spectrum, plus the result of the photon upscattering off these energetic pairs which leads to an extension of the emergent spectrum up to 10 MeV. In that case, the CC temperature is 5 keV ($\dot{m} = 4$). In Figures 11–13 we also demonstrate the general relativity (GR) geometry, photon and pair distributions (spectra) for different radii within the converging flow, respectively.

It is worth noting that similar spectra in the HSS in quite a few BH binaries were observed by the OSSE and COMPTEL instruments [see Grove et al. (1998) and McConnell et al. (1994), respectively]. In particular, seven

BH transient sources, GRO J0422+32, GX 339-4, GRS 1716-249, GRS 1009-45, 4U 1543-47, GRO J1655-40, and GRS 1915+105, observed by OSSE demonstrated two Gamma spectral states (HSS and LHS) and the transition between these two states. [Grove et al. \(1998\)](#) emphasize that, in the LHS, the emergent spectra are characterized by hard spectra with photon indices $\Gamma < 2$ and exponential cut off of energies ~ 100 keV. This form of the spectra is consistent with the thermal Comptonization case [see [Sunyaev & Titarchuk \(1980\)](#)]. These spectra were observed by [Grove et al. \(1998\)](#) for GRO J0422+32, GX 339-4, GRS 1716-249, GRS 1009-45. While GRS 1009-45, 4U 1543-47, GRO J1655-40, and GRS 1915+105 show the high soft state (HSS) with relatively soft photon index, Γ in the range from 2.5 to 3. Furthermore, [Grove et al. \(1998\)](#) have found that the HSS emergent spectrum in GRO J1655-40 is extended to 690 keV without any sign of the rollover at low energies. One can compare this Grove's spectrum with our Monte Carlo simulated HSS spectrum demonstrated in Figure 10.

[McConnell et al. \(1994\)](#) provided details of the Cyg X-1 observations in the 0.75-30 MeV energy range using the COMPTEL instrument in CGRO. They found the Cyg X-1 spectrum in the HSS to be extended at least up to 1 MeV without any break. No physical explanation was suggested to explain this observational result besides a suggestion of incorporating a spectral component which represents the reflection of the hard X-rays from an optically thick accretion disk (see [Hardt & Maraschi \(1993\)](#)). However, this reflection scenario is inconsistent with the soft state emergent Cyg X-1 spectrum because spectra with photon index higher than 2 do not demonstrate the reflection effect. Indeed, the spectrum is too steep and there is not enough photons at high energies to transfer them to lower energies to make a reflection (or downscattering) bump [see [Laurent & Titarchuk \(2007\)](#)]. However, we argue using our simulations that the combined OSSE-COMPTEL spectrum for Cyg X-1 in the HSS demonstrated in [McConnell et al. \(1994\)](#) can result from the Comptonization of the soft (disk) photons by pairs in the converging flow, as shown in Fig. 10.

5. A REDSHIFTED ANNIHILATION RADIATION. A HIGH TEMPERATURE BB (HBB) COMPONENT

[Titarchuk, Seifina & Chardonnet \(2018\)](#), hereafter TSC18 (paper II) found observational evidences of the high temperature BB (HBB) bump around 20 keV, which could be fitted by a ~ 4.5 keV blackbody profile, in black hole accreting systems. Evolutions of spectral characteristics of GRS 1915+105, SS 433 and V4641 Sgr are very similar and all of them reveal the HBB feature which is centered around 20 keV. Using *RXTE* and INTEGRAL data, TSC18 demonstrated that the HBB component is needed in the IS broad-band spectra of SS 433. On the other hand the comparative analysis of the *BeppoSAX* and *RXTE* data shows that flaring pattern for GRS 1915+105 and V4641 Sgr, respectively, demonstrates a transition from the IS to the LHS. It is interesting that the HBB feature is usually observed in the same X-ray luminosity range ($5 \times 10^{36} - 5 \times 10^{37}$ erg/s) for different sources. Thus, one can raise a natural question on the origin of this HBB.

TSC18 estimated the optical depth for photon-photon interaction very close to a BH horizon. In order to do this, they calculated the photon density N_γ near a black hole horizon, assuming that most photons have energy greater than $m_e c^2 = 511$ keV:

$$N_\gamma = \frac{L_\gamma}{4\pi r^2 m_e c^2}, \quad (2)$$

where $L_\gamma \simeq 10^{37}(m/10)$ erg/s, $r_S = 2GM/c^2$ is the Schwarzschild radius, (or $r_S = 3 \times 10^6(m/10)$ cm), c is the speed of light (3×10^{10} cm/s) and the electron rest energy, $m_e c^2$ is about 5×10^{-7} erg. As a result, they obtain that $N_\gamma = 0.6 \times 10^{19}/(M_{bh}/10M_\odot)$ cm $^{-3}$. Then the optical depth for photon-photon interactions can be estimated as

$$\tau_{\gamma-\gamma} \sim \sigma_{\gamma-\gamma} N_\gamma r_S. \quad (3)$$

The cross section for $\gamma - \gamma$ interaction, $\sigma_{\gamma-\gamma} \sim 0.2\sigma_T$, where $\sigma_T = 6 \times 10^{-25}$ cm 2 is the Thomson cross-section. Thus, they find that $\tau_{\gamma-\gamma} \sim (1 - 2)$ using Eqs. (2-3). It is important to emphasize that $\tau_{\gamma-\gamma}$ is independent of the BH mass. We demonstrate in our Monte Carlo simulations (see also TSC18), that the IS luminosity of order 10^{37} erg s $^{-1}$ is sufficient to get a high enough optical depth $\tau_{\gamma-\gamma}$ to trigger photon-photon interaction very close to a BH horizon.

So, pairs (electrons and positrons) are effectively generated as a result of $\gamma - \gamma$ interactions near a BH horizon, within a shell of order of 100 ($M_{bh}/10M_\odot$) m. The generated positrons propagate and may interact with accreting electrons leading to the formation of the annihilation line at 511 keV. A significant fraction of these line photons can directly escape to the Earth observer if the Klein-Nishina optical depth, τ_{KN} at 511 keV is of order of one. In the way out these 511 keV line photons undergo gravitational redshift with z around 20 forming the HBB with color temperature around 20 keV. Observationally this HBB feature has an equivalent width in the interval from 400 to 700 eV (see TSC18, Fig. 9).

As noticed in §4, in the HSS, the dimensionless mass accretion rate is much greater than 1, and the produced pairs and annihilation photons generated near a BH horizon cannot escape, as they are effectively scattered off converging electrons. In the other hand, in the LHS, the converging flow is surrounded by a hot, relatively thick Compton Cloud (CC) with plasma temperature of order of 50-80 keV, and the escaping HBB photons are scattered off hot electrons of the CC and the bump is smeared out. So, it is not by chance that we cannot observe the HBB bump in the HSS when \dot{m} is high (see TSC18, Fig. 9 there) neither in the LHS, but only in the transient IS, where \dot{m} is around 1 – 2. In Fig. 14, we plot the simulated bump equivalent width evolution with \dot{m} .

6. CONCLUSIONS

We made extensive Monte Carlo simulations of X-ray spectral formation in the cloud surrounding a black hole. We found the emergent spectrum extends to relatively high energies up to 400 keV due to up upscattering of the soft (disk) photons illuminating the CC region. Moreover, one can observe a redshifted annihilation line formed near a black hole horizon when the dimensionless mass accretion rate \dot{m} is in the range of 1 – 2 and the plasma temperature kT_e is of order or lower than 5 keV. These conditions are met when a BH is observed in the intermediate state. The annihilation line is formed due the pair production when the upscattered photon energies exceed 511 keV threshold. The generated positrons in their way out annihilate with incoming electrons produce the 511 keV line. This line being produced very close to a BH horizon, the photons undergoes a significant redshift of order of 20 while going out to the Earth observer and the line is observed as an high energy bump around 20 keV.

This annihilation line cannot be observed in the LHS characterized by a low mass accretion rate, less than one, and a hot Compton cloud with plasma temperature about 50 keV surrounding the converging flow site (see Figs. 1 and 14). Moreover, in the HSS, the annihilation line is effectively generated very close to a horizon but the line photons cannot escape as they are scattered in the optically thick converging flow (see Fig. 14). This line is then observed in the IS, as it demonstrated in the accompanying paper (TSC18).

When we take into account the non-linear effect of the positron-electron (pair) generation very close to a BH horizon we find that the surrounding photons upscattered off generated pairs form an additional hard tail extended up to a few MeV (see Fig. 10). It is worth noting that the observed spectra of a few BHs demonstrated this high energy extension [see McConnell et al. (1994), (Grove et al. 1998)] but up to now there were not any reasonable explanation of this phenomenon in the literature.

We should acknowledge the referees efforts on the clear presentation of our paper.

APPENDIX

A. ANALYTICAL DERIVATION OF SOME KEY RESULTS OF THE SIMULATIONS

A.1. *Elements of General Relativity: Photon trajectories in curved space. Lengths and optical paths*

In the flat space, trajectories of unscattered photons is a straight line for which equation can be written in terms of the sinus theorem:

$$r(1 - \mu^2)^{1/2} = \hat{p} \quad (\text{A1})$$

where r is the length of a radius vector \mathbf{r} at a given point of the line, $\mu = \cos\beta$ is the cosine of the zenith angle β between the radius vector \mathbf{r} and the straight line and \hat{p} is the impact parameter of this line. Unscattered photon trajectories in the Schwarzschild background is just a generalization of this sinus theorem (TZ98)

$$\frac{x(1 - \mu^2)^{1/2}}{(1 - 1/x)^{1/2}} = p \quad (\text{A2})$$

where $x = R/R_S$ and $R_S = 2GM/c^2$ is the Schwarzschild radius, $p = \hat{p}/R_S$ and M is a BH mass.

Using equation (A2) we can explain all properties of the photon trajectory in the Schwarzschild background. In other words:

- i. The photon can escape from the black hole horizon to infinity or vice versa for if $p < p_0 = (6.75)^{1/2}$, (see TZ98).
- ii. The photon, for which $p = p_0$, undergoes circular rotation at $x = 1.5$ (at $3GM/c^2$).

- iii. All photons for which $p > p_0$ and $x < 1.5$ are gravitationally attracted by the black hole. In this case all photon trajectories are finite.
- iv. All photons which starts at $x > 1.5$ and have $p > p_0$ escape to infinity if they are not scattered off electrons in the way out.

The photon trajectory can be presented in polar coordinates r and φ . Using the metric of the Schwarzschild background we can write (see Fig. 11) that

$$rd\varphi = \frac{\tan \beta dr}{(1 - 1/x)^{1/2}}. \quad (\text{A3})$$

Then it follows from Eqs.(A2-A3) that

$$\varphi = \int_1^x \frac{d\eta}{\eta^2 \sqrt{1/p^2 - (1 - 1/\eta)/\eta^2}}. \quad (\text{A4})$$

This formula is identical to that derived in [Landau & Linfshitz \(1971\)](#) using the Hamilton-Jacobi (formalism) equation. In fact, the equation of the photon trajectory in polar coordinates readily follows from the sinus theorem (Eq. A2) and the Schwarzschild metric. Equation (A4) is valid for any nonzero p -photon trajectory except a circular one at $x_0 = 3/2$ for which $p_0 = (6.75)^{1/2}$. Formula (A4) should be numerically calculated. From formula (A2) it is evident that $\mu_0 = 1$ at $x_0 = 1$, i.e. the photon always enters to a BH horizon along radial direction.

The length of the radial trajectory($p = 0$) is an integral

$$l = r_S \int_1^x \frac{dx}{(1 - 1/x)^{1/2}}. \quad (\text{A5})$$

For $\alpha = (x - 1) \ll 1$ the length from r_S to r is

$$l \approx 2r_S \alpha^{1/2}. \quad (\text{A6})$$

For $x \gg 1$ we have

$$l \approx r_S x \quad (\text{A7})$$

The Thomson optical path on radial trajectory from r_S to r (or from $x = 1$ to $x = r/r_S$) is

$$T_T(r, r_S) = r_S \int_1^x \sigma_T n_e(\eta) d\eta, \quad (\text{A8})$$

where σ_T is the Thomson cross-section and

$$n_e(r) = \dot{m}(r_S/r)^{1/2}/(2r\sigma_T) \quad (\text{A9})$$

is the electron density [see [Turrola et al. \(2002\)](#) for the derivation of n_e]. The optical path can be found analytically as

$$T_T(r, r_S) = \tau_T(x, 1) = \frac{\dot{m}}{2} \int_1^x \frac{dx}{x^{3/2} \sqrt{1 - 1/x}} = \dot{m}[\pi/2 - \arcsin(1/x)]. \quad (\text{A10})$$

Hence, the total radial Thomson optical depth of the converging flow is

$$\tau_0 = \tau_T(\infty, 1) = (\pi/2)\dot{m}. \quad (\text{A11})$$

For the Thomson optical paths of the finite trajectories entering to BH horizon for which $\alpha = (x - 1) \ll 1$ we have

$$\tau_T(r, r_S) = \sigma_T n(r_S) l \approx \dot{m} \alpha^{1/2}. \quad (\text{A12})$$

A.2. *Pair creation effect near BH horizon. The photon shell*

If the energetic photons have a high number density $n_{ph} \gg 1/(\sigma_T l)$, where l is the characteristic scale of the region within which the Comptonization (in our case the Bulk motion Comptonization) takes place, then the process of electron-pair production by two photons becomes important. Indeed, when a Compton upscattered photon of energy E_1 interacts with another one of energy E_2 , it may produce an electron-positron pair provided their energies satisfy the following relationship:

$$E_1 E_2 > (m_e c^2)^2. \quad (\text{A13})$$

The related cross-section for pair production $\gamma_1 + \gamma_2 \rightarrow e^+ + e^-$ by two photons $\sigma_{\gamma\gamma}$ (Akhiezer & Berestetsky 1965) depends on the product $y = [E_1 E_2 / 2(m_e c^2)^2](1 - \mathbf{\Omega}_1 \mathbf{\Omega}_2)$, where $(E/c)\mathbf{\Omega}$ is the momentum for a given photon of energy E . The cross-section is only nonzero when $y > 1$. The maximum of $\sigma_{\gamma\gamma}(y_{max}) \approx 0.26\sigma_T$ takes place at $y^2 \approx 2$.

The mean energy of the photons upscattered in the converging flow $\langle E \rangle$ (Titarchuk, Mastichiadis & Kylafis 1997)

$$\langle E \rangle = E_0 [1 + 4/\dot{m}]^{N_{sc}} \quad (\text{A14})$$

This formula is obtained without taking into account the gravitational redshift. It presumably works in the part of the converging flow where $(1 - 1/x)^{1/2}$ is of order of unity (namely where $x \gtrsim 1.2$). The mean number of scattering $N_{sc} \sim \dot{m}$. Then $\langle E \rangle / E_0 \sim 16$ and $\langle E \rangle = 24$ keV for $\dot{m} = 4$ and $E_0 = 1.5$ keV. These photons of energy $\langle E \rangle$ when they propagate towards the BH horizon are blueshifted. Their energy increases by a factor

$$\langle E \rangle_{bs} / \langle E \rangle = 1/(1 - 1/x)^{1/2}. \quad (\text{A15})$$

Photon energy of order $m_e c^2 = 511$ keV and higher are achieved in the narrow shell around a BH horizon

$$0 < \alpha = x - 1 < (\langle E \rangle / m_e c^2)^2. \quad (\text{A16})$$

For a given $\langle E \rangle = 24$ keV we obtain that $\alpha < 2.5 \times 10^{-3}$. For 10 solar masses black hole the thickness of the shell is about 70 meters where the pairs can be created due to photon-photon interactions. In Figure 2 we show the average photon energy of Monte Carlo simulated spectrum as a function of radius in converging flow. We assume in this Monte Carlo simulations that the dimensionless accretion rate of the converging flow $\dot{m} = 4$ and the electron temperature $kT_e = 5$ keV. Energy of the injected soft photons is 1.5 keV. As seen from Figure 2, the average photon energy is about 25 keV at radius $R = 1.2R_S$, which is very close to our estimate presented above (see Eq. A14). Also, we can see from this Figure that the blue-shift and Comptonization are equally important below $R = 1.02R_S$.

The photon density in the converging inflow n_{ph} near the BH horizon can be estimated using the photon flux injected in the flow $F_{inj} = L_{inj}/E_0$. Thus

$$n_{ph} \sim \frac{F_{inj}}{4\pi r_S^2 c} = 3 \times 10^{21} (L_{inj}/10^{37} \text{ erg s}^{-1})(m/10)^{-2} (E_0/1.5 \text{ keV})^{-1} \text{ cm}^{-3} \quad (\text{A17})$$

and the free path for the pair creation is

$$l_{\gamma\gamma} \sim (n_{ph} 0.25\sigma_T)^{-1} = 2 \times 10^3 (L_{inj}/10^{37} \text{ erg s}^{-1})^{-1} (m/10)^2 (E_0/1.5 \text{ keV}) \text{ cm}. \quad (\text{A18})$$

The typical length of the photon trajectories l_{cross} in the shell of width α can be estimated using formula (A6)

$$l_{cross} = 2\alpha^{1/2} R_S > 3 \times 10^5 (m/10) \text{ cm} \quad (\text{A19})$$

for $\alpha = 2.5 \times 10^{-3}$. So the shell photons have enough time to create the pairs because

$$t_{cross}/t_{\gamma\gamma} = l_{cross}/l_{\gamma\gamma} \gg 1. \quad (\text{A20})$$

Optical depth for the pair creation is

$$\tau_{\gamma\gamma} = l_{cross}/l_{\gamma\gamma} > 150 (L_{inj}/10^{37} \text{ erg s}^{-1})(m/10)^{-1} (E_0/1.5 \text{ keV})^{-1}. \quad (\text{A21})$$

A.3. The pair spectrum

The spectrum of the pairs created in the photon shell can be calculated using the shell photon spectrum. In Figure 12 we show the Monte-Carlo photon spectra computed for three different radius ranges in the flow. The black histogram is the emergent spectrum seen by observers on Earth. The green histogram is the spectrum seen by observers staying at radial distance $R = (1 - 1.1)R_S$ from the black hole. The blue histogram is the spectrum for observers staying at radial distance $R = (1 - 1.01)R_S$.

As we argue above the pairs have to be created in the shell very close to the horizon. As seen from the shell photon spectrum presented in Figure 12 (blue histogram there) there are a plenty of photons of energy much higher than 511 keV that along with the photons of energies between 10-100 keV (see a bump in the blue histogram) can create a noticeable amount of pairs. The photon spectrum is quite flat, the index of the high energy power-law part being about 1.2 (1.2 ± 0.1). It is worth pointing out that the shape of the spectrum is very close to a broken power-law.

Because of the gravitational blueshift and upscattering the peak of spectrum is located at energy about 25 keV that is 17 times more the energy of the injected soft photons (1.5 keV). The photon index of 1.2 is a typical index for the saturation Comptonization. In fact, the photon index Γ can be calculated (see Titarchuk & Lyubarskij (1995), hereafter TL95; Ebisawa, Titarchuk & Chakrabarti (1996))

$$\Gamma = 1 + \frac{\ln(1/P)}{\ln(1 + \eta)}, \quad (\text{A22})$$

where P is the probability of photon scattering in a cloud (shell) and $1 + \eta = \langle E' \rangle / E$ is a mean efficiency of the photon energy change at any scattering of photon off electrons. According to TL95 (in their notation the scattering probability is λ),

$$1/P = \exp(\beta) = [\tau \ln(1.53/\tau)]^{-1}. \quad (\text{A23})$$

This formula is derived for the plane geometry and $\tau \ll 1$.

In the photon horizon shell the bulk velocity of the flow v is very close to the speed of light $v = c(r/r_S)^{1/2}$. For $R = 1.01R_S$, the Lorentz factor $\gamma = [1 - (v/c)^2]^{-1/2} = 10$. The mean efficiency (see e.g. Pozdnyakov et al (1983))

$$\langle E' \rangle / E = 1 + \eta = [1 + \frac{4}{3}(\gamma^2 - 1)]. \quad (\text{A24})$$

For $\dot{m} = 4$ the shell optical depth $\tau \approx 0.4$ (see Eq. A12). We assume for this estimate that $\alpha = (R - R_S)/R_S = 0.01$. We obtain the photon index $\Gamma \sim 1.13$ using formulae (A22-A24) where we put $\gamma = 10$ and $\tau = 0.4$. This value of $\Gamma = 1.13$ is very close to that, $\Gamma = 1.2 \pm 0.1$, obtained in our MC simulations.

The spectrum of the electrons (positrons), so called the differential yield of the pairs produced by the annihilation of two photons is proportional to the rate of a number of collisions in a given volume (shell). In general terms this rate of number of collisions \dot{N}_{col} is calculated according to Landau & Linfshitz (1971) as follows

$$\dot{N}_{col} = \dot{n}_-(\gamma_-) = C_f c \int_0^\infty n_{ph}(\epsilon_1) d\epsilon_1 \int_0^\infty n_{ph}(\epsilon_2) \sigma(\gamma_-, \epsilon_1, \epsilon_2) d\epsilon_2, \quad (\text{A25})$$

where $\epsilon = E/m_e c^2$ is the dimensionless photon energy, γ_- , γ_+ are the Lorentz factor of the electron/positron, $\sigma(\gamma_-, \epsilon_1, \epsilon_2)$ is the differential cross-section of the pair production cross-section and a factor C_f is less than one.

Formula (A25) is valid for an isotropic radiation field where $\sigma(\gamma_-, \epsilon_1, \epsilon_2)$ is the differential cross-section of the pair production cross-section averaged over a solid angle and $C_f = 1/4$, (see Bottcher & Schlickeiser (1997)). In our MC simulation we implement the exact form of the cross-section where the angular dependence has been included. However, we want to demonstrate that formula (A25) (formally derived for isotropic radiation) can still be applicable for the realistic situation modeled in our simulations.

The exact but quite complicated expression for this formula was derived by Bottcher & Schlickeiser (1997). Now, let us consider the simple approximations of formula (A25) and compare them with that obtained in the simulations.

The first approximation of formula (A25) is related to a δ -function approximation of the cross-section suggested by Zdziarski & Lightman (1985), hereafter ZL85:

$$\sigma(\gamma_-, \epsilon_1, \epsilon_2) \approx \frac{1}{3} \sigma_T \epsilon_2 \delta\left(\frac{\epsilon_1}{2} - \gamma_-\right) \delta\left(\frac{2}{\epsilon_1} - \epsilon_2\right). \quad (\text{A26})$$

To justify this cross-section approximation ZL85 argue that the photons with $\epsilon_1 \gg 1$ will produce e^+e^- pairs mostly with $\gamma_- \approx \gamma_+ \approx \epsilon/2$ (Bonometto & Rees (1971)) while colliding with photons of energies of $\epsilon_2 \approx 2/\epsilon_1$ (Herterich (1974)).

Integration in formula (A25) using equation (A26) leads to

$$\dot{n}_-(\gamma_-) \propto c\sigma_T \frac{1}{\gamma_-} n_{ph}(1/\gamma_-) n_{ph}(2\gamma_-). \quad (\text{A27})$$

Γ_{pair} should be around of 2.5 because the photon index of $n_{ph}(1/\gamma_-)$ is about 0.5 for $1/\gamma_- \ll 1$ and that of $n_{ph}(2\gamma_-)$ is around 1 (see Fig. 12). In Figure 13 we present the simulation results for pair energy distribution. As one can see the simulated pair spectrum is well approximated by a power law of index 2.5.

REFERENCES

- Akhiezer, A. & Berestetsky, V 1965, Quantum Electrodynamics, New York; Interscience
- Bonometto S. & Rees M.J., 1971, MNRAS, 152, 21
- Borozdin, K., Revnivtsev, M., Trudolyubov, S., Shrader, C. & Titarchuk, L. 1999, ApJ, 517, 367
- Bottcher, M. & Schlickeiser, R., 1997, A&A, 325, 866
- Di Salvo T., Stella L., Robba N.R. et al., 2000, ApJ, 544, L119
- Ebisawa K., Titarchuk L., and Chakrabarti S.K., 1996, PASJ, 48, 59
- Farinelli, R. & Titarchuk, L. 2011, A&A, 525, 102
- Grove, J.E., Johnson, W.N, Kroeger, R.A, McNaron-Brown, K., Skibo, J.G. & Philips, B.F. 1998, ApJ, 500, 899
- Haardt, F. & Maraschi, L. 1993, ApJ, 413, 507
- Herterich K., 1974, Nature, 250, 311
- Hua, X-M. & Titarchuk, L. 1995, ApJ, 449, 188
- Landau, L.D.& Linfshitz, E.M. 1971, The classical theory of fields. New York: Pergamon Press
- Laurent, P. & Titarchuk, L. 2011, ApJ, 727, 34
- Laurent, P. & Titarchuk, L. 2007, ApJ, 656, 1056
- Laurent, P. & Titarchuk, L. 2001, ApJ, 562, L67 (LT01)
- Laurent, P. & Titarchuk, L. 1999, ApJ, 511, 289 (LT99)
- McConnell, M. 1994, ApJ, 424, 933
- Moskalenko I.V., & Jourdain E., 1997, A&A, 325, 401
- Pozdnyakov, L.A., Sobol', I.M. & Sunyaev R.A. 1983, Astrophys. Space. Phys. Rev., 9, 1
- Seifina, E. & Titarchuk, L. 2011, ApJ, 738, 128
- Shakura, N.I., & Sunyaev, R.A., 1973, A&A, 24, 337 (SS73)
- Shaposhnikov, N. & Titarchuk, L. 2009, ApJ, 699, 453
- Sunyaev, R.A. & Titarchuk, L.G. 1980, A&A, 86, 121
- Svensson, R. 1982, ApJ, 258, 335
- Titarchuk L. & Lyubarskij Y. 1995, ApJ, 450, 876
- Titarchuk, L., Seifina, E. & Frontera 2013, ApJ, 767, 160
- Titarchuk, L. & Shaposhnikov, N. 2010, ApJ, 724, 1147
- Titarchuk L. & Zannias T. 1998, ApJ, 493, 863 (TZ98)
- Titarchuk, L. G., Mastichiadis, A., & Kylafis, N. D. 1997, ApJ, 487, 834
- Titarchuk, L., Seifina, E. & Chardonnet P. 2018, ApJ, submitted (TSC18)
- Turolla, R., Zane, S., & Titarchuk, L. 2002, ApJ, 576, 349
- Zdziarski A.A & Lightman A.P., 1985, ApJ, 294, L79

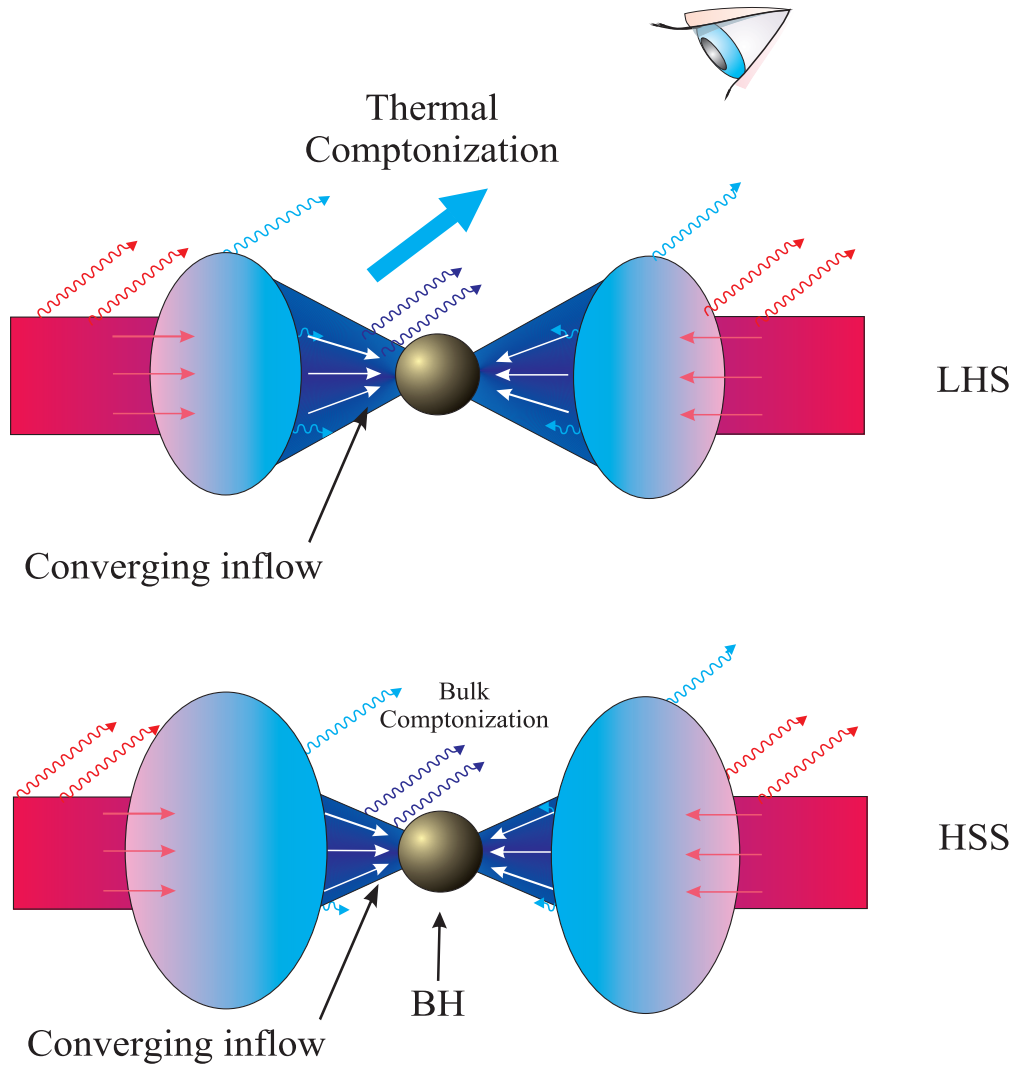


Figure 1. Geometry of a black hole binary. We present two corresponding panels for the low/hard state (LHS) and for the high/soft state (HSS).

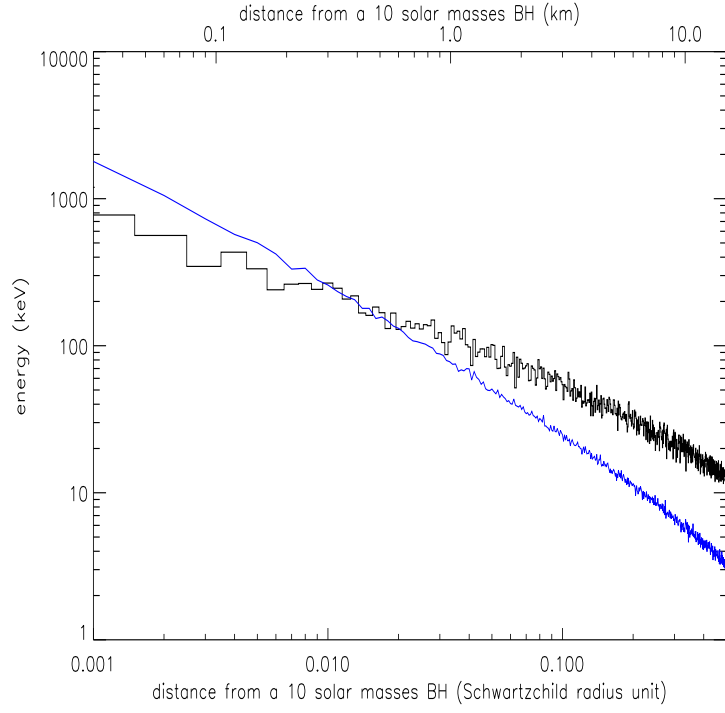


Figure 2. Average photon energy of the upscattered photons (black histogram) and blue-shifted energy of injected soft photon (blue line) as a function of radius.

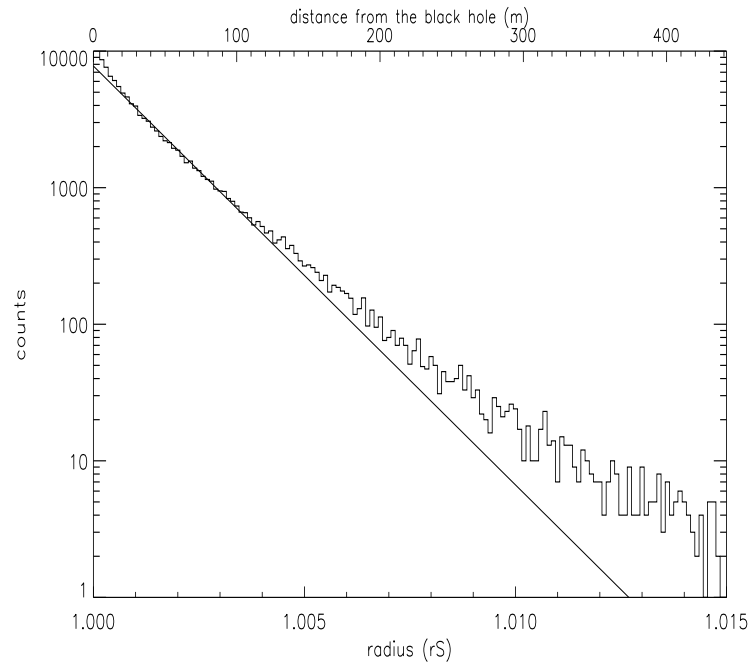


Figure 3. Number density profile of the created pairs as a function of radius.

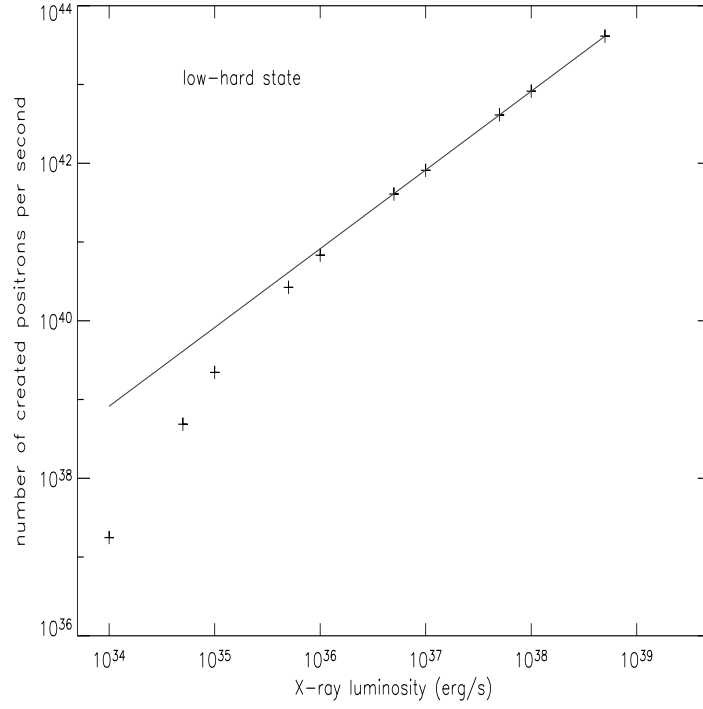


Figure 4. Number of created positrons for a given X-ray luminosity of the source in the low-hard state ($kT_e = 50$ keV, $\dot{m} = 2$).

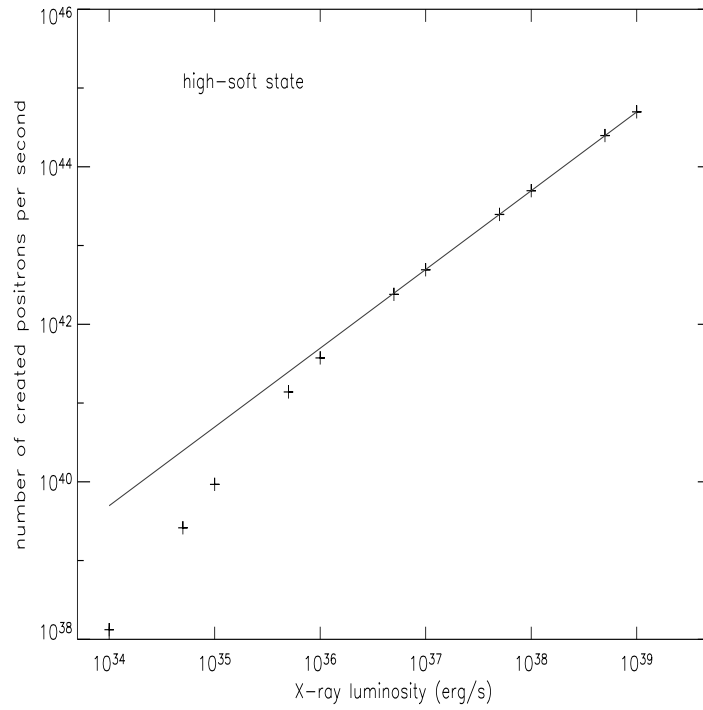


Figure 5. Number of created positrons for a given X-ray luminosity of the source in the high-soft state ($kT_e = 5$ keV, $\dot{m} = 4$).

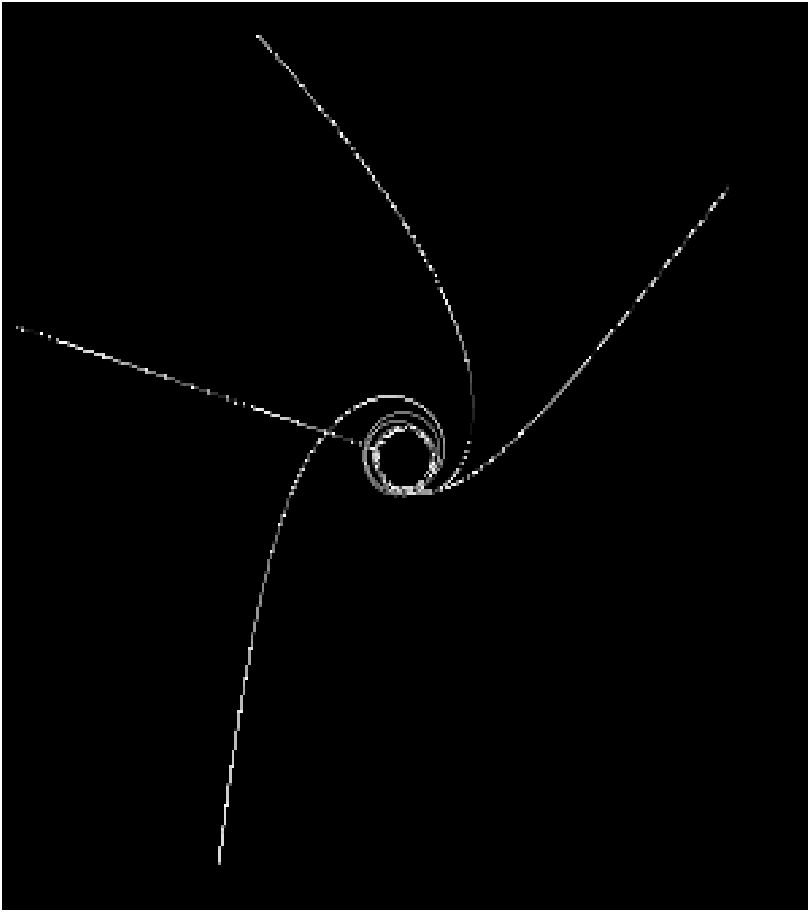


Figure 6. Trajectories of the created positrons in the Schwarzschild background. Only a few positrons among the 5×10^5 simulated here can reach $3r_S$. This number is even lower if we take into account Coulomb losses and annihilation at the positrons (see text)

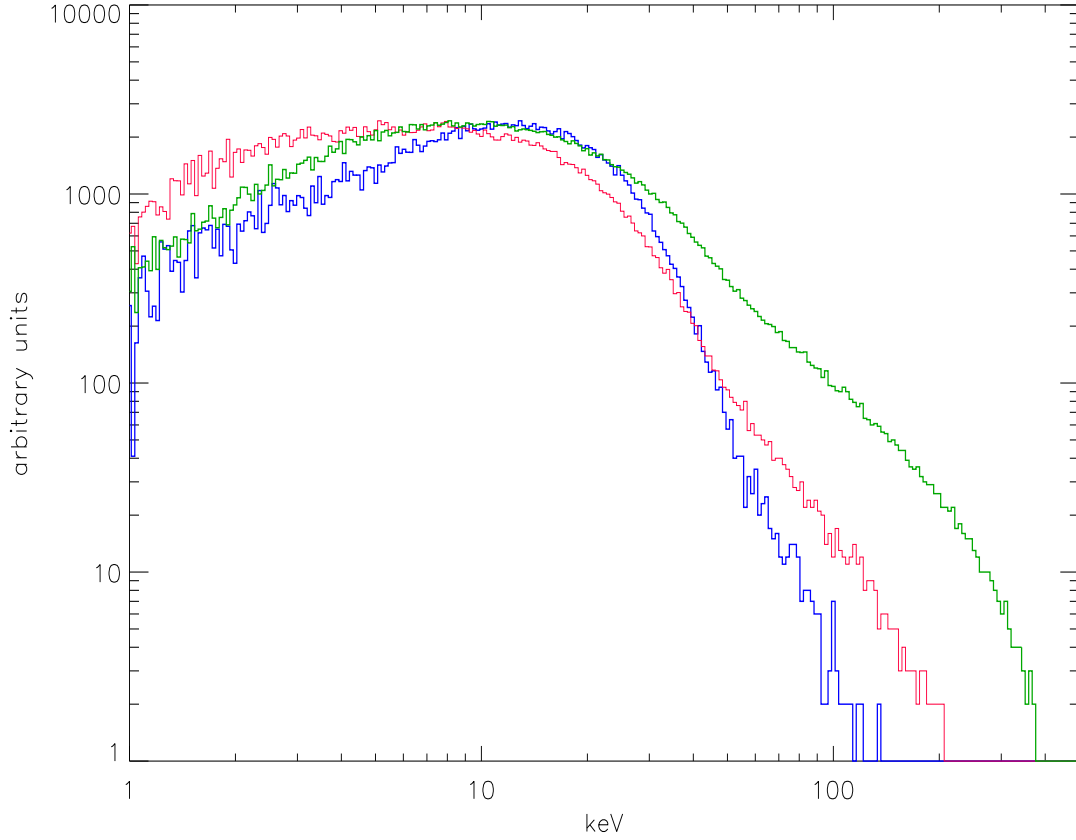


Figure 7. Emergent photon spectrum of the annihilated positrons. As the 511 keV emission from annihilation is produced at different radius from a BH, the line endure different redshift, thus producing a continuum. In these set of simulations, the temperature of the CC was 5 keV and its density was varied from \dot{m} equal to 1 (blue line), 4 (red line), and 10 (green line). The main component of the spectra seems not to change much with \dot{m} , but a hard component rises when \dot{m} increases. Due to the concurring effects of the pair creation efficiency and CC opacity to the 511 keV radiation, the spectrum is maximum for intermediate $\dot{m} = 4$. The fit of the $\dot{m} = 1$ spectrum with a blackbody spectral shape ($kT = 6.2$ keV) is shown by a dashed line.

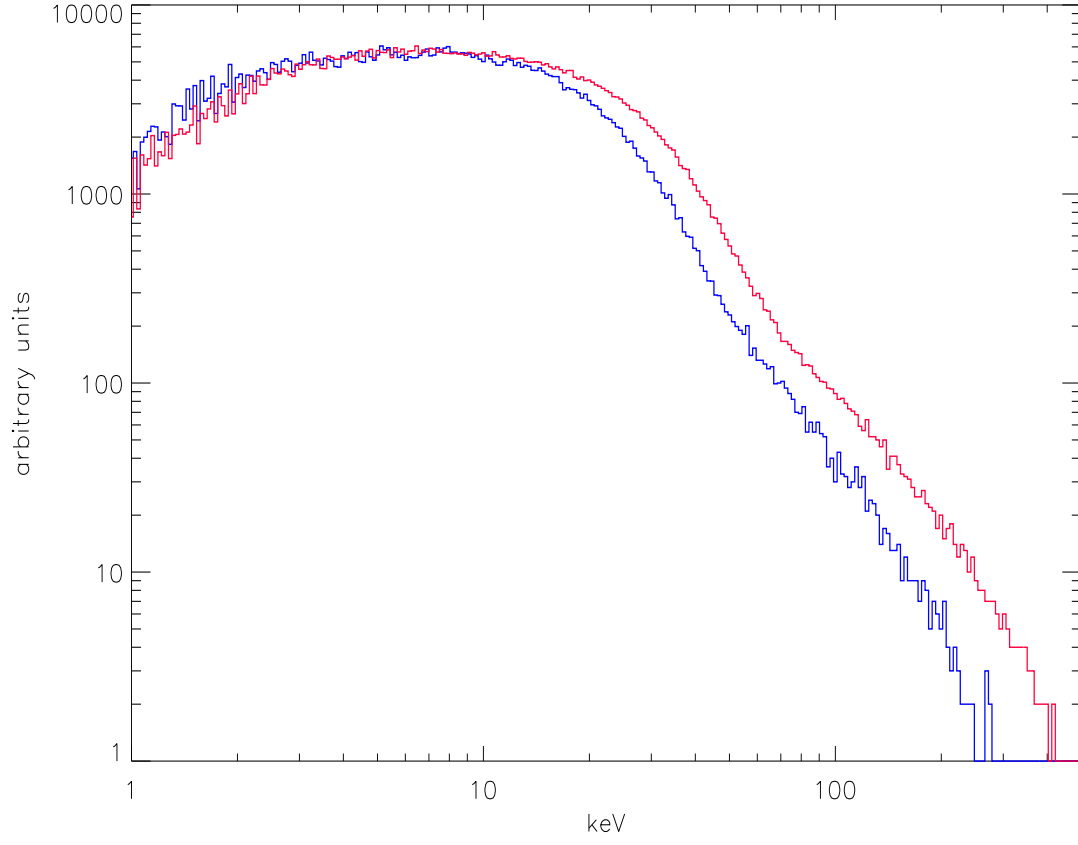


Figure 8. Emergent photon spectrum of the annihilated positrons. In these set of simulations, \dot{m} equals to 4 and CC electron temperatures are 5 keV (blue line) and 50 keV (red line). The cutoff energy of this annihilation line spectrum only slightly changes with the cloud temperature. The fit of the $\dot{m} = 4$ spectrum with a blackbody spectral shape ($kT = 6.4$ keV) is shown by a dashed line.

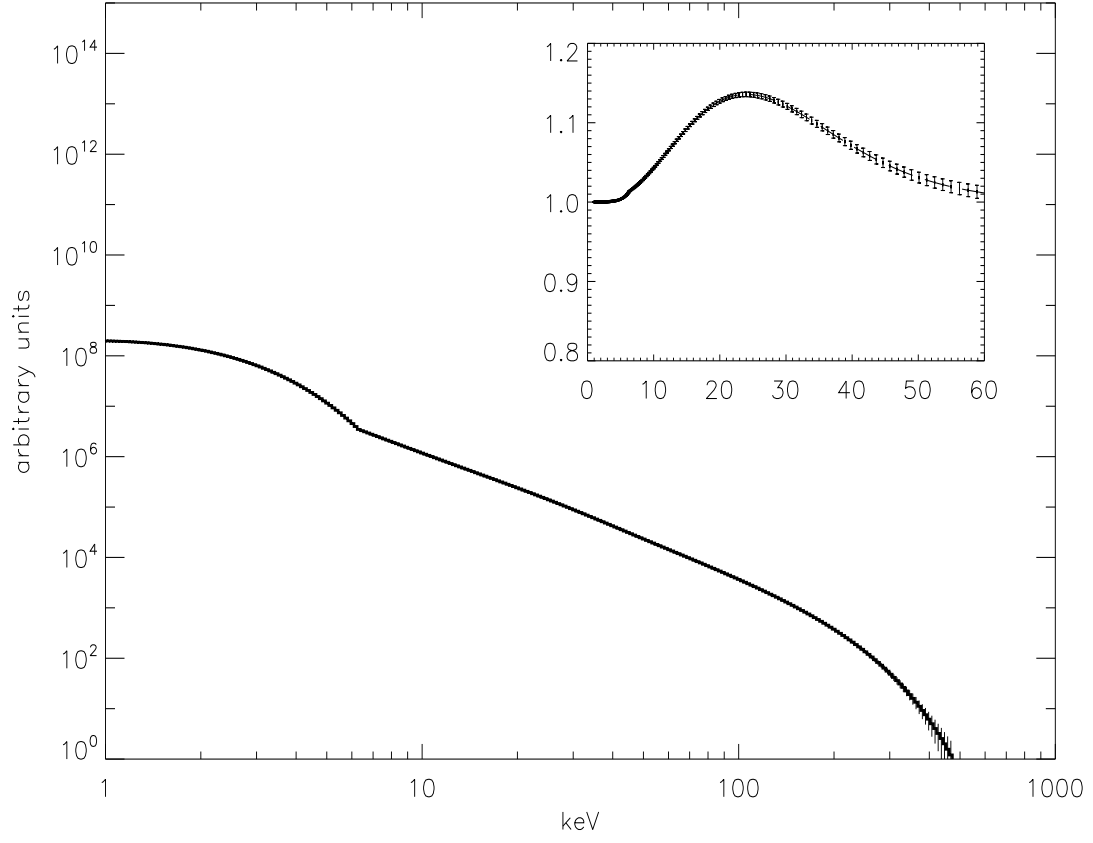


Figure 9. Emergent photon spectrum which includes a gravitationally redshifted annihilated line. On the upper encapsulated right-hand panel we include the redshifted annihilation line as a ratio of the resulting spectral values to the Comptonized continuum.

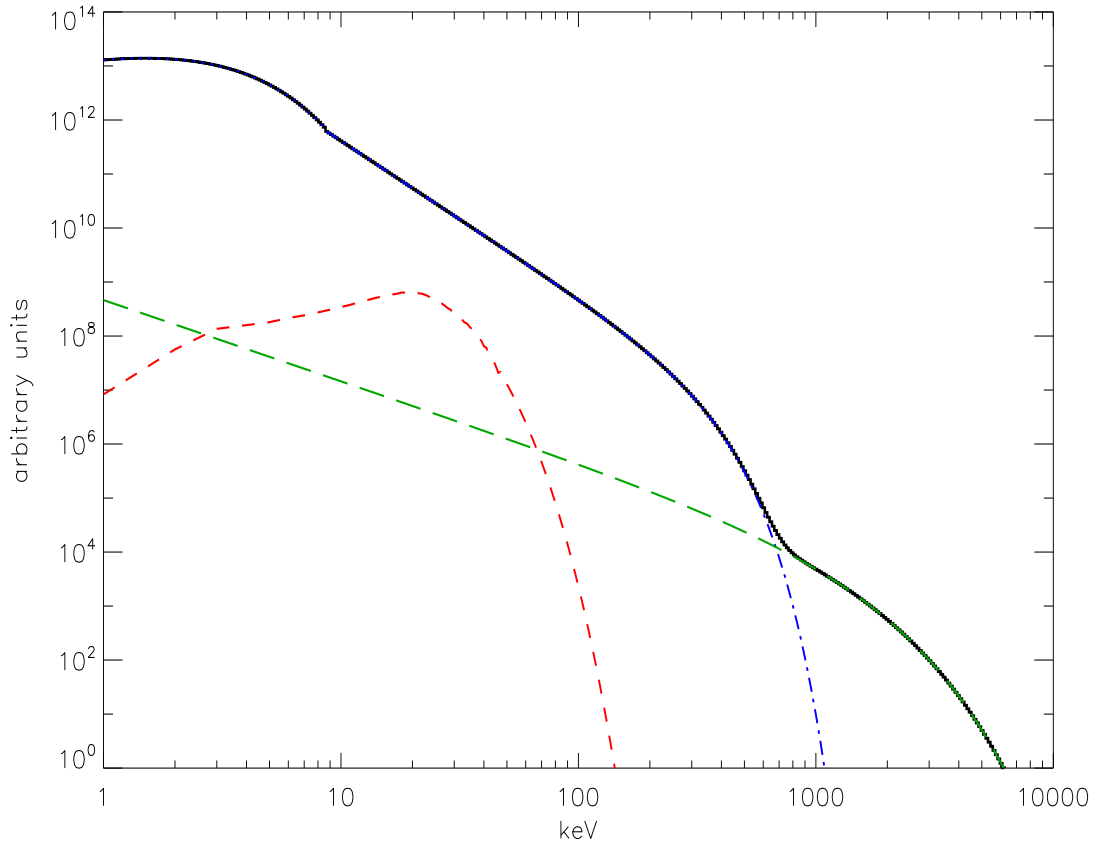


Figure 10. Spectrum at infinity resulting from the redshifted pair annihilation line (red) the Comptonization of X-ray photons on the CC electrons (blue) and Comptonization on created pairs (blue). In that case, the CC temperature is 5 keV ($\dot{m} = 4$).

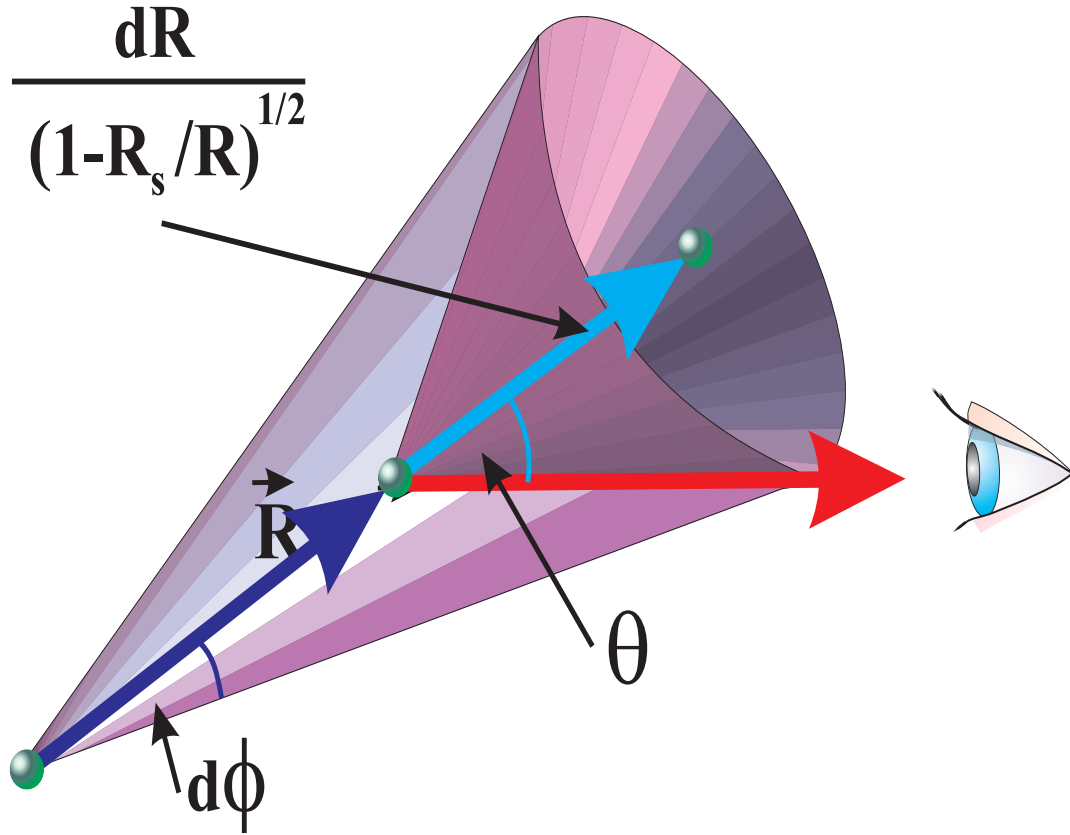


Figure 11. Sketch of light propagation in the Schwartzchild metric.

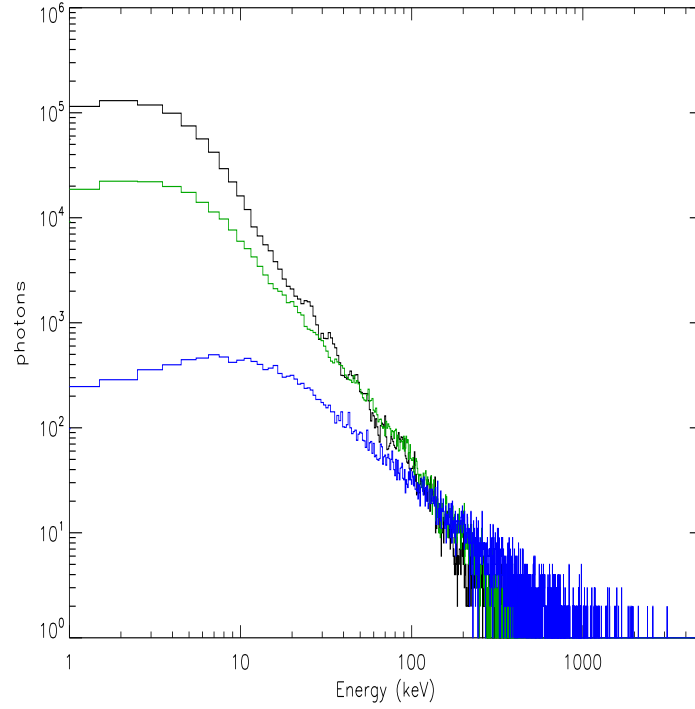


Figure 12. The photon spectra for three different radius ranges in the flow. The black histogram is the emergent spectrum seen by observers on Earth. The green histogram is the spectrum seen by observers staying at radial distance $R = (1 - 1.1)R_S$ from the black hole. The blue histogram is the spectrum for observers staying at radial distance $R = (1 - 1.01)R_S$.

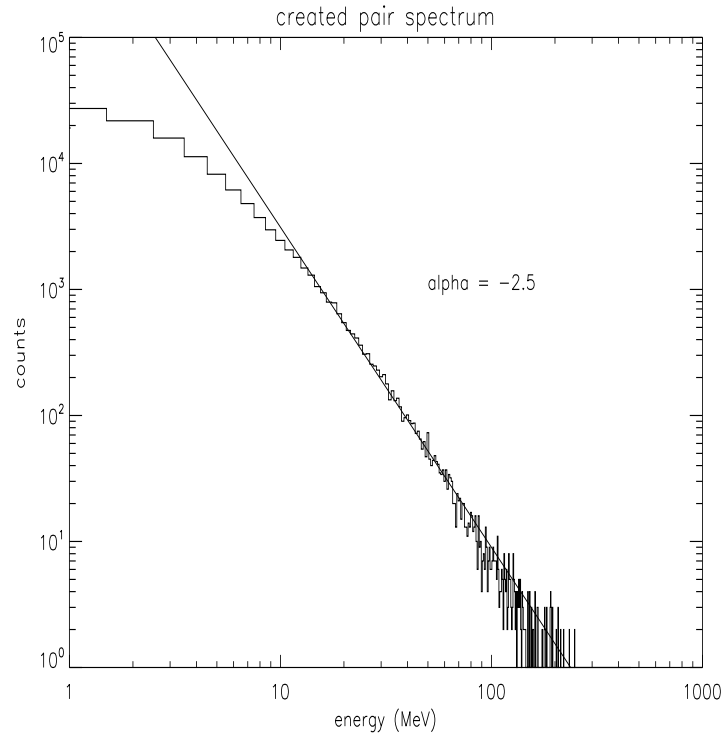


Figure 13. Spectrum of the created pairs. Solid line is the best-fit of the simulated histogram by a power law which index is 2.5.

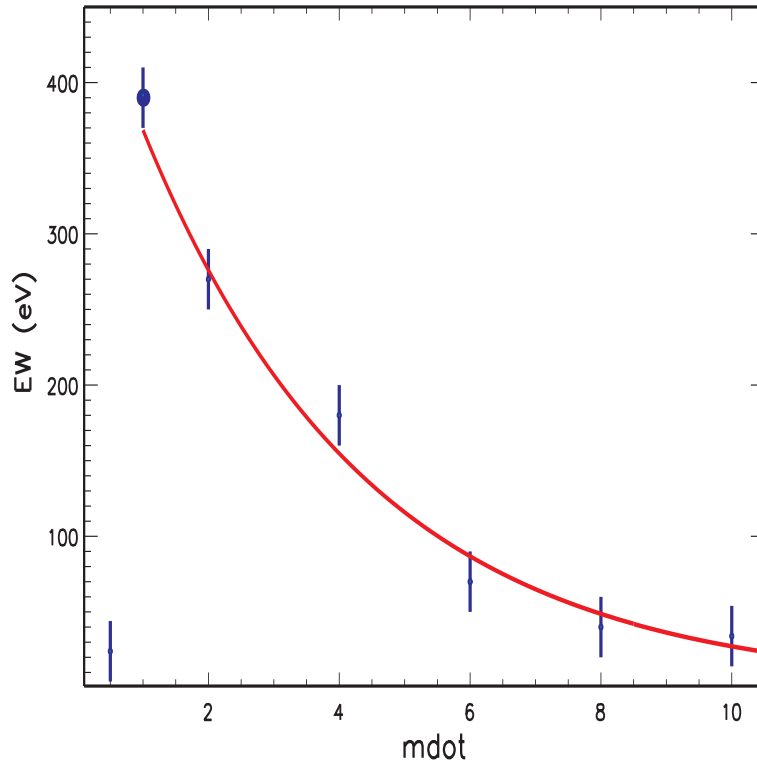


Figure 14. Evolution of the pair bump with the mass accretion rate \dot{m} . We measured the bump strength by computing its equivalent width (EW). Due to the concurring effects of the pair creation efficiency and CC opacity to the 511 keV radiation, the EW is maximum for a limited range of \dot{m} (see text).